



Antiferromagnetic domain wall dynamics in magnetoelectric MnTiO₃ studied by optical imagingTatsuki Sato , Nobuyuki Abe,^{*} Yusuke Tokunaga, and Taka-hisa Arima*Department of Advanced Materials Science, University of Tokyo, Kashiwa 277-8561, Japan* (Received 13 September 2021; revised 17 February 2022; accepted 23 February 2022; published 14 March 2022)

We study the dynamics of the antiferromagnetic domain wall in collinear antiferromagnet MnTiO₃ by means of optical magnetochiral imaging. Antiphase domains are clearly visualized by exploiting the asymmetry in absorption coefficients between two distinct antiferromagnetic states with Néel vectors in opposite directions. Utilizing the coexistence of several types of magnetic multipoles, antiferromagnetic states in MnTiO₃ are switched by longitudinal DC electric and magnetic fields applied along the propagation direction of incident light while imaging the domain pattern. The memory effect enables the imaging of millisecond dynamics with domain inversion. Detailed investigation of the domain-wall motion with varying temperature and external-field strength reveals the thermal effects on the mobility of the domain wall.

DOI: [10.1103/PhysRevB.105.094417](https://doi.org/10.1103/PhysRevB.105.094417)**I. INTRODUCTION**

In magnetic materials, macroscopic magnetic properties such as the magnetization \mathbf{M} and magnetic susceptibility are often dominated by the positions and dynamics of magnetic domain boundaries. Real-space imaging is one of the most powerful techniques to study the domain pattern. Considering the recently growing interest in antiferromagnets characterized by the Néel vector \mathbf{L} by virtue of the zero stray field and fast dynamics [1,2], a fundamental understanding of antiferromagnetic domain patterns and domain-wall motion based on imaging techniques is of particular importance.

Domain observation is more difficult in antiferromagnets than in ferromagnets, where magnetic circular dichroism enables the visualization of domains [3]. Compared with scanning probe microscopies [4–6], synchrotron-radiation imaging techniques [7–10], and spatially resolved magnetothermal measurements [11,12], the optical imaging of antiferromagnetic domain patterns [13–23] is characterized by simple implementation and a large millimeter-scale field of view. The second harmonic generation of light has been established as a successful tool to visualize domains in several antiferromagnets [15–20]. However, the nonlinear optical process requires long-time irradiation with a light beam of a high photon density, which often causes a temporal resolution worse than a few minutes and specimen heating.

The use of the multipole-induced linear magneto-optic effect in antiferromagnets is a promising approach to reduce the long exposure time, as suggested by recent imaging studies utilizing the octupole-induced magneto-optical Kerr effect [21] and quadrupole-induced nonreciprocal linear dichroism [23]. One may think that the interaction between odd-parity magnetic multipoles in antiferromagnets and electromagnetic fields also offers clues for the control of \mathbf{L} using external

fields [24,25]. In fact, visible multipoles that interact with a transverse electromagnetic wave do not inherently couple to the DC electric and magnetic fields (\mathbf{E} and \mathbf{H}) parallel to the propagation direction \mathbf{k} of light. For conducting an imaging study of the field-driven motion of antiferromagnetic domains, thin plates of antiferromagnets, where \mathbf{L} is controllable with $\mathbf{E} \parallel \mathbf{k}$, are suitable for applying a high electric field while retaining a large field of view.

Magnetochiral dichroism (MCHD) is a linear magneto-optic effect with which we can observe the spatial distribution of the magnetic toroidal moment \mathbf{T} [24]. MnTiO₃ is a collinear antiferromagnet in which \mathbf{T} coexists with magnetic monopole and quadrupole moments [26,27]. In MnTiO₃, the direction of \mathbf{T} is in one-to-one correspondence with that of \mathbf{L} [27]. A diagonal term in magnetoelectric (ME) coupling allows the control of \mathbf{L} using electric and magnetic fields in the $\mathbf{E} \parallel \mathbf{H} \parallel \mathbf{k}$ configuration (Fig. 1). Here, we report an imaging study of the antiferromagnetic domain structure of MnTiO₃ using MCHD. The antiphase domain structure in MnTiO₃ is clearly visualized by exploiting the asymmetry in absorption coefficients between two distinct antiferromagnetic states with opposite \mathbf{L} directions. The MCHD-based imaging technique is independent of the polarization direction of light. Furthermore, both quasistatic and dynamic motions of antiferromagnetic domain walls in driving electric and magnetic fields are captured.

II. ME COUPLING IN MnTiO₃

MnTiO₃ crystallizes in the ilmenite structure with the space group $R\bar{3}$ [28]. Buckled honeycomb layers consisting of Mn²⁺ with $S = 5/2$ and those of nonmagnetic Ti⁴⁺ are alternately stacked along the c axis in a hexagonal setting. Both Mn²⁺ and Ti⁴⁺ are octahedrally coordinated by six oxygen ions. Each unit cell contains four formula units. Below the Néel temperature $T_N = 65$ K, MnTiO₃ adopts easy-axis collinear antiferromagnetic ordering without doubling the unit cell [29,30]. The magnetic symmetry $\bar{3}'$ allows the linear ME

^{*}Present address: Department of Physics, College of Humanities and Sciences, Nihon University, Tokyo 156-8550, Japan.

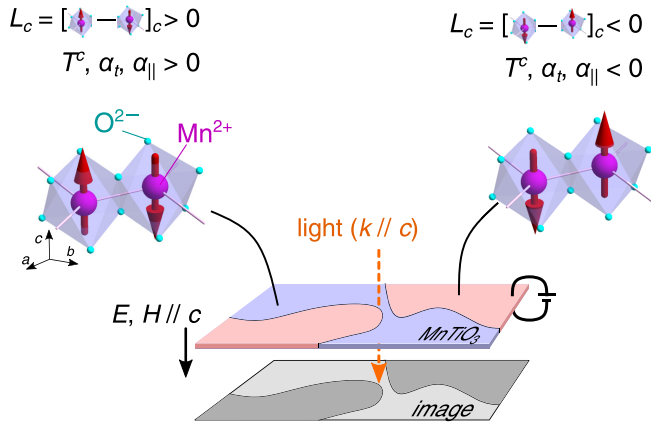


FIG. 1. Schematic of antiferromagnetic domain imaging in MnTiO_3 . The red arrows represent $S = 5/2$ spins of Mn^{2+} . The antiferromagnetic domain pattern is mapped as the difference in the transmitted light intensity. Signs of the c component of the toroidal moment and all the components of the ME tensor α are opposite between the two types of antiferromagnetic domains with L_c of opposite signs. Exploiting the diagonal ME coupling α_{\parallel} , L_c is manipulated by external DC electric and magnetic fields parallel to the propagation direction of light.

tensor [26,27]

$$\alpha = \begin{pmatrix} \alpha_{\perp} & \alpha_t & 0 \\ -\alpha_t & \alpha_{\perp} & 0 \\ 0 & 0 & \alpha_{\parallel} \end{pmatrix}. \quad (1)$$

Antiferromagnetic domains of opposite L should host α of opposite signs. In the presence of a fixed magnetic field, two types of antiferromagnetic domains host P_{ME} in opposite directions. Hence, the degeneracy between the two states is lifted by the simultaneous application of H and E . The energy gap is expressed as $|2\alpha H \cdot E|$ ($\equiv |2\mathcal{F}_{\text{ME}}|$), which may drive domain walls. Since $|\alpha_{\parallel}|$ is larger than $|\alpha_{\perp}|$ and $|\alpha_t|$ for MnTiO_3 in a wide temperature range [27], we focus on the diagonal response α_{\parallel} in Eq. (1) to drive domain walls.

III. METHODS

Single crystals of MnTiO_3 were grown by the floating zone method in Ar flow. Grown crystals were cut into plates with large c planes. Each plate was thinned to 0.1–0.15 mm. The crystal plate was cooled down in a ^4He closed-cycle refrigerator. The optical measurements were performed at a photon energy $\hbar\omega = 2.16$ eV, where the largest MCHD signal was observed [27]. Monochromatized light from a halogen lamp was propagated along the c axis of the crystal. The transmitted light was detected by a charge-coupled detector camera (Alta U6, Apogee Instruments). To reduce the influence of roughness of the crystal surfaces, a reference image without domain patterns was subtracted from each image [31]. Gold with a thickness of 17.5 nm was sputtered onto both c planes to form electrodes for applying an electric field along the c axis. Electric and magnetic fields were applied using a high-voltage supply (Model 2657A, Keithley) and an electromagnet, respectively.

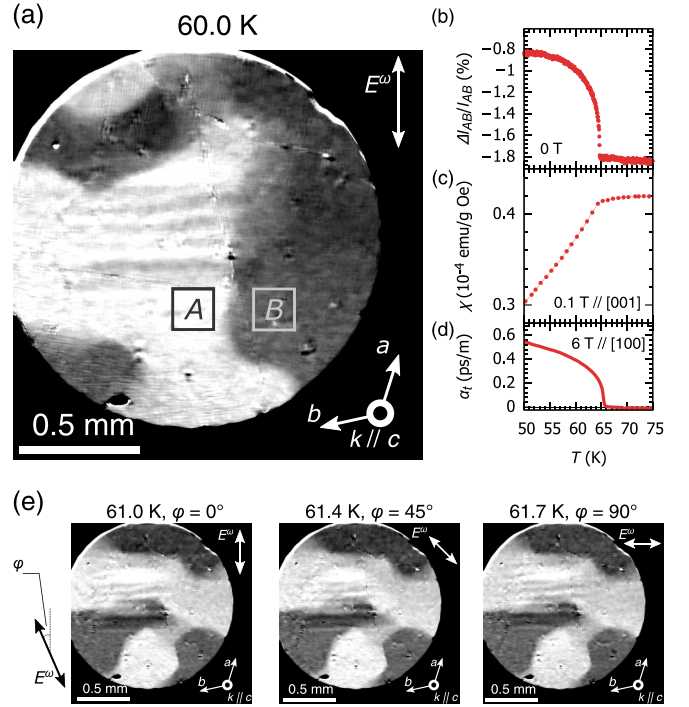


FIG. 2. (a) Difference image at 60.0 K. An image at 65.0 K is used as the reference. The exposure time is 2 s. (b) Temperature dependence of the relative difference $\Delta I_{AB}/I_{AB}$ in the integrated intensity between square regions A and B indicated in (a) at 0 T. (c) Temperature dependence of the magnetic susceptibility χ along the easy axis. (d) Temperature dependence of the DC ME susceptibility α_t calculated using magnetic-field induced electric polarization in 6 T [see Eq. (1) in the text]. (e) Light-polarization dependence of difference images. Images at 65.0 K ($\varphi = 0^\circ$), 65.4 K ($\varphi = 45^\circ$), and 65.7 K ($\varphi = 90^\circ$) are used as the reference. The data for (d) are from Ref. [27].

IV. RESULTS AND DISCUSSION

A. MCHD-based imaging of domain pattern

Figure 2(a) shows a difference image of a MnTiO_3 crystal without gold electrodes at 60 K in a warming procedure without any external fields. Before the experiment, the crystal was cooled down from 120 to 3 K in the absence of external fields. Then, images were collected as the crystal was warmed. The temperature sweeping rate around 60 K was 0.6 K/min. A pronounced domain pattern arises in the circular field of view. The origin of contrast in Fig. 2(a) is investigated through the temperature dependence of the difference in transmitted light intensity between brighter and darker regions. The relative difference in brightness is defined as $\Delta I_{AB}/I_{AB} = (I_A - I_B)/(I_A + I_B)$. Here, $I_{A(B)}$ is the average intensity of the area A (B) and is computed as $I_{A(B)} = \int_{A(B)} d\mathbf{r} I(\mathbf{r}) / \int_{A(B)} d\mathbf{r}$. $I(\mathbf{r})$ denotes the transmitted light intensity at a pixel position \mathbf{r} in a frame at each temperature before subtracting the reference image. $\int_{A(B)} d\mathbf{r}$ denotes the integral over a square labeled A (B) in Fig. 2(a). $\Delta I_{AB}/I_{AB}$ values of approximately -1.8% above T_N , where magnetic domains disappear, are attributable to the contribution of the inhomogeneous distribution of incident light and the sample thickness. $\Delta I_{AB}/I_{AB}$ increases as the temperature decreases below T_N , as shown in Fig. 2(b).

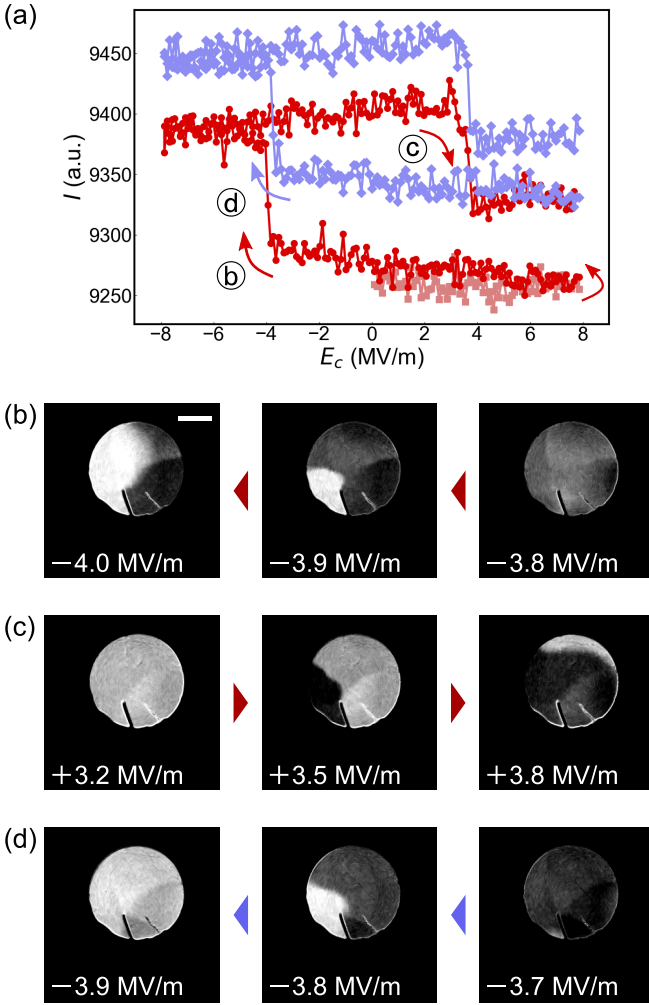


FIG. 3. (a) Change in the averaged transmitted light intensity I with a sweeping electric field E_c along the c axis. (b)–(d) Difference c -plane images recorded at each electric field. The panels in (b), (c), and (d) were recorded during the first decrease, second increase, and second decrease in E_c . Images at $E_c = -7.9$ MV/m in the first loop, $E_c = 7.9$ MV/m at the end of the first loop, and $E_c = -7.9$ MV/m in the second loop are used as the reference for (b), (c), and (d), respectively. The white scale bar in the left panel of (b) corresponds to 0.5 mm.

The temperature dependence of the magnetic susceptibility χ along the c axis and the antisymmetric component of the ME coupling tensor α_t are shown in Figs. 2(c) and 2(d), respectively. Figures 2(b)–2(d) clearly evidence the magnetic origin of the contrast in Fig. 2(a). The magnetically induced change in $\Delta I_{AB}/I_{AB}$ at 55 K in Fig. 2(b) is as large as 1%, corresponding to the magnitude of MCHD signal at 2.16 eV in MnTiO₃ [27].

Figure 2(e) shows domain images obtained with linearly polarized incident light beams of several polarization directions φ . All the images were taken without any fields in series in an identical warming run, which was different from that of Fig. 2(a). The obtained images are independent of φ , agreeing with the nature of MCHD as the directional dichroism of unpolarized light. Hence, we conclude that the antiferromagnetic domain patterns in Figs. 2(a) and 3 are of MCHD origin.

Typically observed domains in MnTiO₃ are of submillimeter scale, which is larger than the specimen thickness. Similarly to Cr₂O₃, domain patterns do not reflect the threefold symmetry of underlying crystals [15].

B. Quasistatic domain inversion

Figure 3 shows the quasistatic switching of antiferromagnetic domains in MnTiO₃ at 64.0 K. Before the measurement, the sample was cooled down from 70 to 64.0 K in the absence of external fields. At 64.0 K, a magnetic field $\mu_0 H_c = 0.1$ T was applied, following which E_c was ramped up from 0 to 7.9 MV/m. E_c was swept between ± 7.9 MV/m for two more cycles. In Fig. 3(a), the averaged transmitted light intensity $I = \int dr I(\mathbf{r}) / \int dr$ shows hysteresis loops with a temporal drift. The result clearly indicates that the darker antiferromagnetic state with a larger absorption coefficient is favored when $E_c H_c > 0$.

The switching process for the first loop of E_c is shown in Figs. 3(b) and 3(c). In Fig. 3(b), a monodomain state at $E_c = -3.8$ MV/m becomes a multidomain state at $E_c = -3.9$ MV/m. The brighter region is expanded by decreasing E_c to -4.0 MV/m, clearly evidencing a motion of the antiferromagnetic domain wall in MnTiO₃ that is driven by electric and magnetic fields. The switching process is similar for an E_c -increasing run. In Fig. 3(c), a monodomain state at 3.2 MV/m becomes a multidomain state at 3.5 MV/m, and the darker region expands with increasing E_c . Both figures show that the domain inversion is dominated by the domain-wall motion, as in other multiferroics [18–20,23], but not by a coherent rotation of magnetic moments. A comparison of Figs. 3(b) and 3(c) reveals that the switching processes in the E_c -increase and E_c -decrease runs are slightly asymmetric; while the coercive electric field is 4 MV/m for both cases, switching with increasing E_c is not as steep as that with decreasing E_c , where a monodomain state persists up to -3.8 MV/m.

The transient state in the second loop of E_c is similar to that in the first loop, indicating a certain memory effect in the isothermal and quasistatic switching. The multidomain state realized at -3.8 MV/m in Fig. 3(d) is similar to that at -3.9 MV/m in the first loop in Fig. 3(b). The striking similarity indicates the presence of an energetically favored pathway for the domain-wall motion. Such a memory effect is often regarded as a consequence of the pinning effect [18].

C. Dynamic switching of domain

The deterministic nature of the domain inversion process enables the investigation of the dynamic switching of antiferromagnetic domains by the repetitive imaging of domain patterns. As shown in Fig. 4(a), each cycle of the measurement in $\mu_0 H_c = 0.1$ T consists of the following three parts. First, a negative electric field $E_c = -7.9$ MV/m is applied for 3 s for poling. Second, a positive pulsed electric field of $E_c = 7.9$ MV/m is applied for time Δt . The electric field is then turned off. Finally, the domain image is recorded at zero electric field. Since the driving force $\mathcal{F}_{ME} = \alpha \mathbf{H} \cdot \mathbf{E}$ per unit area against a domain wall is zero in the absence of the electric field, a domain pattern exactly at time Δt after the abrupt

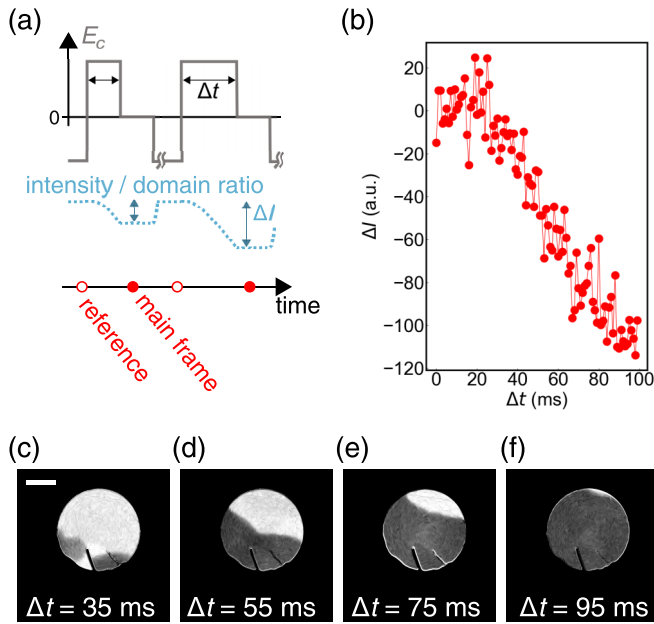


FIG. 4. (a) Timing scheme of the experiment. Reference images were recorded in every poling process. All the measurements were performed under $\mu_0 H_c = 0.1$ T. The averaged transmitted light intensity (blue dotted line) takes the maximum value after poling with the negative voltage and decreases by ΔI in response to the application of the positive pulsed electric field for Δt . (b) The change in the transmitted light intensity ΔI compared with each reference image at 64 K as a function of Δt . (c)–(f) Difference images recorded after the application of a positive pulsed field of several pulse widths Δt [31]. The white bar in (c) corresponds to 0.5 mm.

switching of E_c from -7.9 to 7.9 MV/m is recorded in the third step. The temporal evolution of the domain pattern in the inversion process is controlled via Δt . The overall picture of the inversion dynamics can be grasped by collecting images with varying Δt .

Figure 4(b) shows the Δt dependence of a change ΔI in the averaged transmitted light intensity with the application of a pulsed electric field at 64.0 K. A pulsed positive electric field of a width $\Delta t \geq 30$ ms results in a smaller I in main frames in comparison with reference images. Antiferromagnetic domains are almost completely switched at $\Delta t = 90$ ms, as inferred from Fig. 3(a), where a steep change in I is observed at the domain inversion. The gradual drop in ΔI for $30 < \Delta t < 90$ ms corresponds to transient states, where the darker region expands in response to the application of a positive electric field. The pulsed electric field with shorter Δt retains the intensity I . Such inactiveness in the beginning of the switching process is indicative of switching dynamics dominated by domain-wall displacement [32,33].

Figures 4(c)–4(f) show difference images acquired after applying a pulsed electric field with several values of Δt . The darker region in the field of view continuously expands with increasing Δt . The millisecond dynamics in the antiferromagnetic domain-wall motion driven by DC electric and magnetic fields in magnetoelectric MnTiO₃ is clearly captured. Note that the antiferromagnetic domain is poled back after every

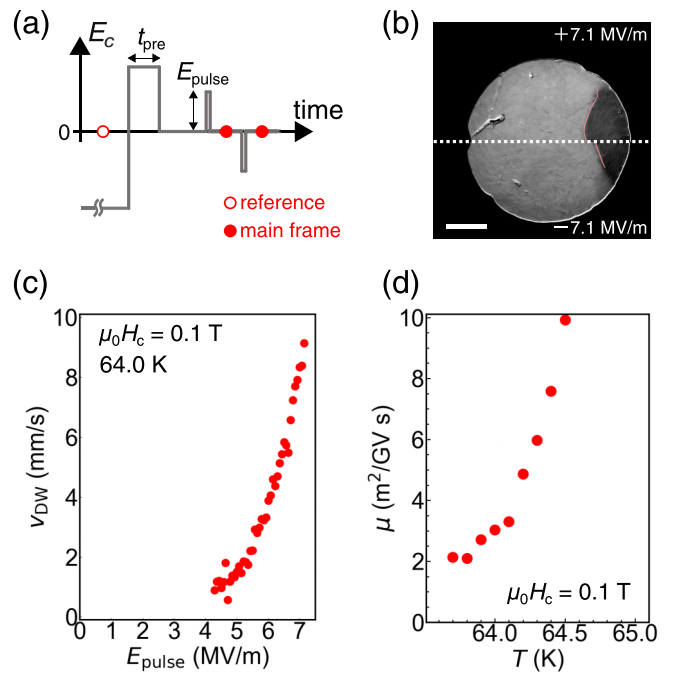


FIG. 5. (a) Timing scheme of the experiment to study the domain-wall dynamics. Each reference image was recorded in the poling process. (b) Comparison of difference images recorded after the application of positive and negative pulsed electric fields with amplitude $E_{\text{pulse}} = 7.1$ MV/m. Before the application of the pulsed field, a multidomain state was realized with a t_{pre} of 450 ms. The position of the domain wall is denoted by a red line. The white bar corresponds to 0.5 mm. (c) Relationship between the domain-wall velocity v_{DW} and the pulse height E_{pulse} of the driving electric field, $v_{\text{DW}}-E_{\text{pulse}}$, at 64.0 K. Measurements were performed for the same multidomain state as was realized for (b). (d) Temperature dependence of the mobility μ of the domain wall in the viscous regime. Measurements were performed for a multidomain state realized with a t_{pre} of 400 ms.

exposure, which indicates the existence of a memory effect in the inversion process. The nearly complete monodomain state in Fig. 4(f) shows a monodomain ferroaxial state over the field of view [31].

Next, we performed a similar measurement with a multidomain initial state to evaluate domain-wall dynamics. Figure 5(a) shows the timing scheme of the experiment. All the measurements are performed in $\mu_0 H_c = 0.1$ T. Prior to the experiment, at 64 K, a negative electric field $E_c = -7.1$ MV/m is applied for poling, following which a positive pulsed electric field with amplitude $E_c = 5.7$ MV/m is applied for time t_{pre} to realize a multidomain state. To investigate the domain-wall velocity v_{DW} , two images are recorded in each cycle: one after the application of a positive pulsed electric field with amplitude E_{pulse} for $t_{\text{pulse}} = 10$ ms and the other after the application of a negative pulsed electric field with the same amplitude for the same duration [see Fig. 5(b)]. v_{DW} is simply estimated by dividing the shift in position of the domain wall between the two images by t_{pulse} . Figure 5(c) shows the E_{pulse} dependence of v_{DW} at 64.0 K. v_{DW} grows with increasing E_{pulse} . Judging from the almost linear

$v_{\text{DW}}-E_{\text{pulse}}$ relationship above $E_{\text{pulse}} = 6$ MV/m, the domain wall is depinned, and its motion is in the viscous regime [34]. For $E_{\text{pulse}} < 6$ MV/m, the domain wall is in the creep regime.

The domain-wall mobility μ is estimated by fitting v_{DW} in the viscous regime to the phenomenological relationship $v_{\text{DW}} = \mu(E_{\text{pulse}} - E_p)$, where E_p denotes the pinning electric field. Figure 5(d) shows the temperature dependence of μ . A divergent enhancement in μ is observed as the temperature approaches T_N . In Ref. [35], by incorporating the ME terms in the antiferromagnetic Lagrangian, the μ in a moderate electric field is given as $\mu \propto (\lambda\alpha_{\parallel}H_c)/(\alpha_0\mathcal{J})$, where λ , α_0 , and \mathcal{J} denote the domain-wall thickness, Gilbert damping parameter, and angular momentum density on one sublattice, respectively. Assuming $\alpha_{\parallel} \propto \mathcal{J}$ [26] and α_0 to be independent of temperature, the enhancement of μ might be ascribed to the growth of λ close to T_N . While the v_{DW} value of 8.3 mm/s in $E_{\text{pulse}} = 7$ MV/m at 64.0 K in MnTiO₃ [Fig. 5(c)] is five orders smaller than in ferroelectric BaTiO₃ in the same electric field [36], the mobility per energy gap between two distinct domains $\mu/(\alpha_{\parallel}\mu_0H_c) = 4.7 \times 10^{-2}$ m⁴/Js in MnTiO₃ is comparable with that in BaTiO₃ of 10^{-3} m⁴/Js. Toward faster domain-wall motion, stronger E_c and H_c [37] as well as a reduction in pinning energy near the spin-flip transition, where the effective magnetic anisotropy is small [38], might be useful.

V. CONCLUSION

We report an MCHD-based imaging study of the antiferromagnetic domain pattern and dynamics in a collinear antiferromagnet MnTiO₃. Submillimeter-scale domain patterns are obtained in difference images. Exploiting the memory effect with domain inversion, we captured both quasistatic and dynamic motions of the antiferromagnetic domain wall that are driven by electric and magnetic fields. It is worth noting that, in antiferromagnets with several magnetic symmetries including tetragonal $\bar{4}'$ and $4/m'$ and hexagonal $\bar{6}'$ and $6/m'$, the ME tensor is expressed by Eq. (1), which is the key to the MCHD-based imaging of the domain-wall motion driven by external fields along the propagation vector of incident light. Our findings indicate a feasible approach for the MCHD-based imaging of antiferromagnetic domains, which can be applied to the study of dynamics in multiferroic domain walls.

ACKNOWLEDGMENTS

We thank T. Kurumaji for valuable comments on the manuscript. This work was partly supported by JSPS KAKENHI Grants No. 18H04309, No. 19H01835, and No. JP19H05826. T.S. is supported by JSPS through the Program for Leading Graduate Schools (MERIT) and a Grant-in-Aid for JSPS Fellows (JSPS KAKENHI Grant No. JP21J13003).

-
- [1] V. Baltz, A. Manchon, M. Tsoi, T. Moriyama, T. Ono, and Y. Tserkovnyak, *Rev. Mod. Phys.* **90**, 015005 (2018).
- [2] P. Němec, M. Fiebig, T. Kampfrath, and A. V. Kimel, *Nat. Phys.* **14**, 229 (2018).
- [3] S.-W. Cheong, M. Fiebig, W. Wu, L. Chapon, and V. Kiryukhin, *npj Quantum Mater.* **5**, 3 (2020).
- [4] M. Bode, E. Vedmedenko, K. Von Bergmann, A. Kubetzka, P. Ferriani, S. Heinze, and R. Wiesendanger, *Nat. Mater.* **5**, 477 (2006).
- [5] P. Schoenherr, L. M. Giraldo, M. Lilienblum, M. Trassin, D. Meier, and M. Fiebig, *Materials* **10**, 1051 (2017).
- [6] P. Appel, B. J. Shields, T. Kosub, N. Hedrich, R. Hübner, J. Faßbender, D. Makarov, and P. Maletinsky, *Nano Lett.* **19**, 1682 (2019).
- [7] J. Stöhr, A. Scholl, T. J. Regan, S. Anders, J. Lüning, M. R. Scheinfein, H. A. Padmore, and R. L. White, *Phys. Rev. Lett.* **83**, 1862 (1999).
- [8] P. G. Evans, E. D. Isaacs, G. Aeppli, Z. Cai, and B. Lai, *Science* **295**, 1042 (2002).
- [9] H. Ueda, Y. Tanaka, Y. Wakabayashi, and T. Kimura, *Phys. Rev. B* **98**, 134415 (2018).
- [10] M. G. Kim, H. Miao, B. Gao, S.-W. Cheong, C. Mazzoli, A. Barbour, W. Hu, S. Wilkins, I. K. Robinson, M. Dean *et al.*, *Nat. Commun.* **9**, 5013 (2018).
- [11] H. Reichlova, T. Janda, J. Godinho, A. Markou, D. Kriegner, R. Schlitz, J. Zelezny, Z. Soban, M. Bejarano, H. Schultheiss *et al.*, *Nat. Commun.* **10**, 5459 (2019).
- [12] T. Janda, J. Godinho, T. Ostatnicky, E. Pfitzner, G. Ulrich, A. Hoehl, S. Reimers, Z. Šobáň, T. Metzger, H. Reichlova, V. Novak, R. P. Campion, J. Heberle, P. Wadley, K. W. Edmonds, O. J. Amin, J. S. Chauhan, S. S. Dhesi, F. Maccherozzi, R. M. Otxoa *et al.*, *Phys. Rev. Mater.* **4**, 094413 (2020).
- [13] N. Kharchenko, V. Eremenko, and L. Belyi, *JETP Lett.* **29**, 392 (1979).
- [14] N. Kharchenko, *Ferroelectrics* **162**, 173 (1994).
- [15] M. Fiebig, D. Fröhlich, G. Sluyterman v. L, and R. Pisarev, *Appl. Phys. Lett.* **66**, 2906 (1995).
- [16] M. Fiebig, T. Lottermoser, D. Fröhlich, A. V. Goltsev, and R. V. Pisarev, *Nature (London)* **419**, 818 (2002).
- [17] B. B. Van Aken, J.-P. Rivera, H. Schmid, and M. Fiebig, *Nature (London)* **449**, 702 (2007).
- [18] T. Hoffmann, P. Thielen, P. Becker, L. Bohat, and M. Fiebig, *Phys. Rev. B* **84**, 184404 (2011).
- [19] A. S. Zimmermann, D. Meier, and M. Fiebig, *Nat. Commun.* **5**, 4796 (2014).
- [20] M. Matsubara, S. Manz, M. Mochizuki, T. Kubacka, A. Iyama, N. Aliouane, T. Kimura, S. L. Johnson, D. Meier, and M. Fiebig, *Science* **348**, 1112 (2015).
- [21] T. Higo, H. Man, D. B. Gopman, L. Wu, T. Koretsune, O. M. van't Erve, Y. P. Kabanov, D. Rees, Y. Li, M.-T. Suzuki *et al.*, *Nat. Photonics* **12**, 73 (2018).
- [22] J. Xu, C. Zhou, M. Jia, D. Shi, C. Liu, H. Chen, G. Chen, G. Zhang, Y. Liang, J. Li, W. Zhang, and Y. Wu, *Phys. Rev. B* **100**, 134413 (2019).
- [23] K. Kimura, T. Katsuyoshi, Y. Sawada, S. Kimura, and T. Kimura, *Commun. Mater.* **1**, 39 (2020).
- [24] N. A. Spaldin, M. Fiebig, and M. Mostovoy, *J. Phys.: Condens. Matter* **20**, 434203 (2008).

- [25] F. Thöle, A. Keliri, and N. A. Spaldin, *J. Appl. Phys.* **127**, 213905 (2020).
- [26] N. Mufti, G. R. Blake, M. Mostovoy, S. Riyadi, A. A. Nugroho, and T. T. M. Palstra, *Phys. Rev. B* **83**, 104416 (2011).
- [27] T. Sato, N. Abe, S. Kimura, Y. Tokunaga, and T.-h. Arima, *Phys. Rev. Lett.* **124**, 217402 (2020).
- [28] K. Kidoh, K. Tanaka, F. Marumo, and H. Takei, *Acta Crystallogr. Sect. B* **40**, 329 (1984).
- [29] G. Shirane, S. Pickart, and Y. Ishikawa, *J. Phys. Soc. Jpn.* **14**, 1352 (1959).
- [30] H. Yamauchi, H. Hiroyoshi, M. Yamada, H. Watanabe, and H. Takei, *J. Magn. Magn. Mater.* **31**, 1071 (1983).
- [31] See Supplemental Material at <http://link.aps.org/supplemental/10.1103/PhysRevB.105.094417> for a detailed description about image processing and the ME tensor components and the axial degree of freedom, which includes Refs. [39,40].
- [32] E. Fatuzzo, *Phys. Rev.* **127**, 1999 (1962).
- [33] M. Labrune, S. Andrieu, F. Rio, and P. Bernstein, *J. Magn. Magn. Mater.* **80**, 211 (1989).
- [34] A. Kirilyuk, J. Ferré, V. Grolier, J. Jamet, and D. Renard, *J. Magn. Magn. Mater.* **171**, 45 (1997).
- [35] K. D. Belashchenko, O. Tchernyshyov, A. A. Kovalev, and O. A. Tretiakov, *Appl. Phys. Lett.* **108**, 132403 (2016).
- [36] W. J. Merz, *Phys. Rev.* **95**, 690 (1954).
- [37] Y. Shiratsuchi, H. Yoshida, Y. Kotani, K. Toyoki, T. V. A. Nguyen, T. Nakamura, and R. Nakatani, *APL Mater.* **6**, 121104 (2018).
- [38] F. Kagawa, M. Mochizuki, Y. Onose, H. Murakawa, Y. Kaneko, N. Furukawa, and Y. Tokura, *Phys. Rev. Lett.* **102**, 057604 (2009).
- [39] J. Hlinka, J. Privratska, P. Ondrejko, and V. Janovec, *Phys. Rev. Lett.* **116**, 177602 (2016).
- [40] L. D. Barron, *Molecular Light Scattering and Optical Activity* (Cambridge University Press, Cambridge, 2009).